Published by IOP Publishing for Sissa Medialab

Received: *January 20, 2020*
Accepted: *March 3, 2020*
Published: *April 6, 2020*

TECHNICAL REPORT

A position sensitive scintillation detector using a side-by-side GAGG-F/GAGG-T phoswich block

Q. Wei,[a] **N. Jiang,**[b] **T. Xu,**[b] **Z. Lyu,**[c] **T. Ma**[c,1] **and Y. Liu**[c]

[a] *Beijing Engineering Research Center of Industrial Spectrum Imaging, School of Automation and Electrical Engineering, University of Science and Technology Beijing, Beijing 100083, China*
[b] *Beijing Novel Medical Equipment Ltd., Beijing 102206, China*
[c] *Department of Engineering Physics, Tsinghua University, Beijing 100084, China*

E-mail: maty@tsinghua.edu.cn

Abstract: Position sensitive detectors are the key component of gamma-ray imaging systems such as coded-aperture cameras and emission computed tomography systems. Improving the intrinsic spatial resolution of detectors is critical to system performances. Recent advance of the GAGG scintillator production allows variable decay time with different Al/Ga ratios. In this paper, we developed a novel position sensitive scintillation detector using a side-by-side fast-GAGG/typical-GAGG (GAGG-F/GAGG-T) phoswich array, which consisting of 12×12 phoswich unit pairs assembled by the GAGG-F scintillator (decay time constant ~ 50 ns) and the GAGG-T scintillator (decay time constant ~ 90 ns) in a pixel size of 1.35×2.7×4 mm^3 and coupled to a 8×8 SiPM (MicroFJ-30035-TSV) array. An experiment was conducted using the irradiation of a ^{57}Co source (122 keV). Experimental results demonstrate that events from the GAGG-F and GAGG-T scintillators can be discriminated with only 7% mis-assignment probability. The 12×12 of GAGG-F and GAGG-T scintillator arrays are both distinguishable in separated flood maps. The average energy resolutions of GAGG-F and GAGG-T scintillators at 122 keV are 27.58% and 23.51% respectively. The side-by-side GAGG-F/GAGG-T detector has the advantage of improved intrinsic spatial resolution, no intrinsic background radiation and uniform detection efficiency.

Keywords: Gamma detectors (scintillators, CZT, HPGe, HgI etc); Scintillators, scintillation and light emission processes (solid, gas and liquid scintillators)

[1]Corresponding author.

https://doi.org/10.1088/1748-0221/15/04/T04001

2020 JINST 15 T04001

Contents

2020 JINST 15 T04001

1 Introduction

Gamma-ray imaging systems [1–8] such as coded-aperture cameras [1–3], and emission computed tomography systems (ECT) [4–6] have been used in many areas such as homeland security [1–3], nuclear medicine [4–6], and radiation therapy [7, 8], et al. Of which, the key component is the position sensitive detector. Driven by the demanding from high quality imaging, detectors with high intrinsic spatial resolution are anticipated. Recently, with the development and improvement of silicon photomultipliers (SiPMs) with advantages of small pixel size, high photon detection efficiency, low operating voltage and so on [9, 10], one promising detector approach is assembling pixelated scintillators with SiPM arrays instead of photomultiplier tube (PMT) arrays [6, 10].

To further improve the position decoding capability, the phoswich techniques using side-by-side phoswich scintillators were explored [11–14]. The phoswich design requires using scintillators with different decay time constants. A side-by-side LYSO/GAGG phoswich scintillator block was developed in our previous study [14]. However, the LYSO scintillator containing ^{176}Lu has background radiation, which will introduce noise events [15]. Although ^{176}Lu background radiation may not significantly influence the performance of common ECT applications [4, 16, 17], however, it reduces the imaging quality and restricts the application in low-activity imaging [18–20].

GAGG is a promising scintillator for gamma-ray detectors [21–24], which has advantages of high density, high Z-effective number, high light yield, relatively fast decay time, non-hygroscopic and no intrinsic radiation. More interestingly, GAGG scintillator can have different decay times with different Al/Ga ratios [25, 26]. Base on this property, a side-by-side GAGG phoswich scintillator detector is proposed in this paper, which can be utilized to build high spatial resolution gamma-ray imaging systems. Details of the prototype detector are demonstrated in the following sections.

2 Materials & methods

2.1 Phoswich detector design

The GAGG phoswich scintillator block (EPIC-Crystal Inc., Shanghai, China) built with 12×12 phoswich unit pairs has a total size of 33.7×33.7×4 mm^3, as shown in figure 1. Reflectors (3M-ESR) are set between phoswich pairs. Each phoswich pair is assembled by gluing a fast-GAGG (GAGG-F) scintillator and a typical-GAGG (GAGG-T) scintillator, both with a size of 1.35×2.7×4 mm^3. Table 1 lists parameters of GAGG-F and GAGG-T scintillators. The phoswich scintillator block is readout by a home-made sparse 8×8 SiPM array (MicroFJ-30035-TSV, SensL). To improve scintillation light collection for the sparse SiPM array, the gaps between the SiPMs are covered by 3M-ESR reflectors [27]. Three signals including X, Y, and E for position decoding and energy retrieved are generated by a 64-channel application specific integrated circuit (ASIC) with in-chip resistor networks [28]. The pulse waveforms of X, Y, and E are digitized with a sampling rate of 65 MHz by a 12-bit analog-to-digital (ADC) chip (AD9637), and then transferred to a PC for off-line studies.

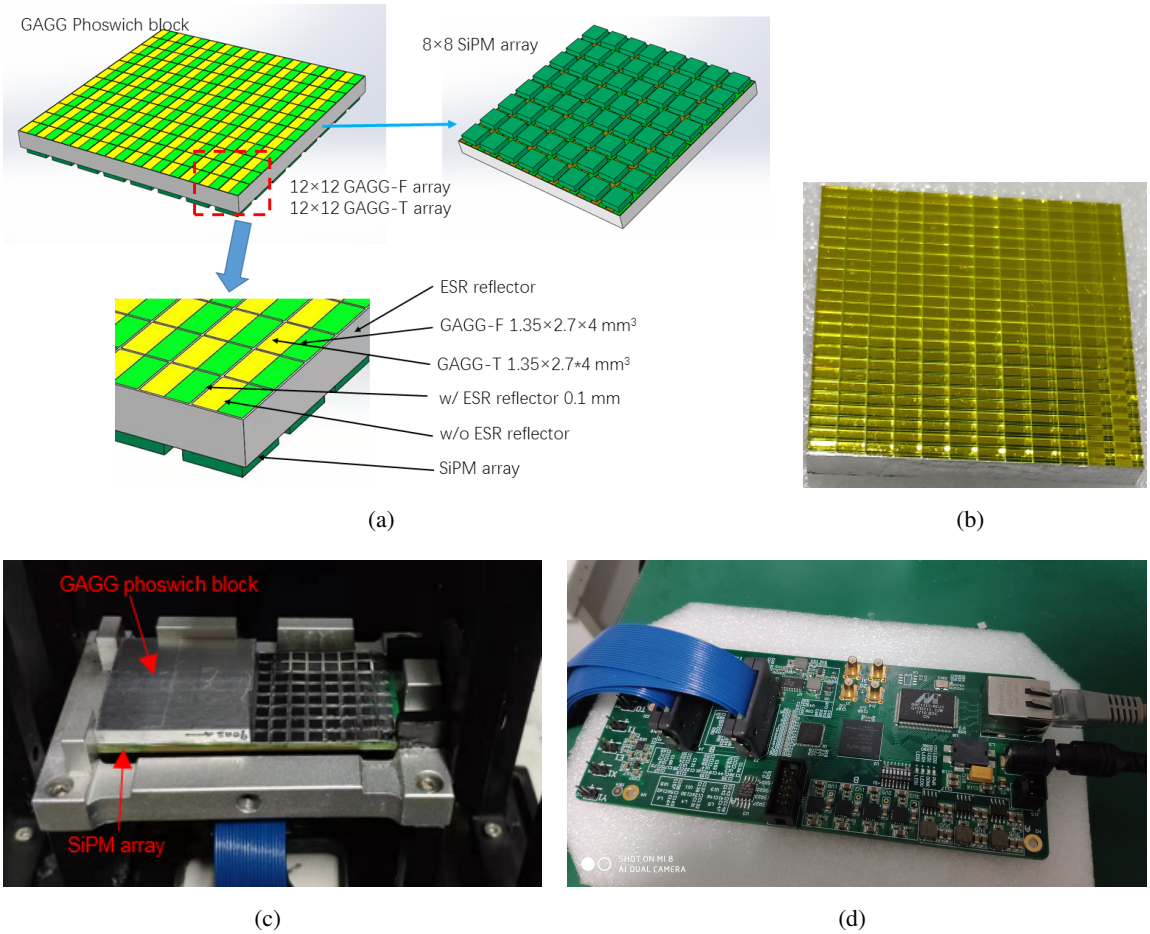

Figure 1. The proposed phoswich scintillator detector: (a) configuration of the side-by-side GAGG-F/GAGG-T phoswich scintillator detector; (b) the GAGG-F/GAGG-T phoswich array, (c) the phoswich scintillator array readout by a spare SiPM array; (d) the acquisition board.

2020 JINST 15 T04001

Table 1. Parameters of the scintillators [29].

Scintillator	Decay time constant (ns)	Light output photons (MeV)	Density (g/cm^3)	Peak emission wavelength (nm)	Reflective index
GAGG-F	50	30000	6.6	520	1.91
GAGG-T	90	42000	6.6	530	1.91

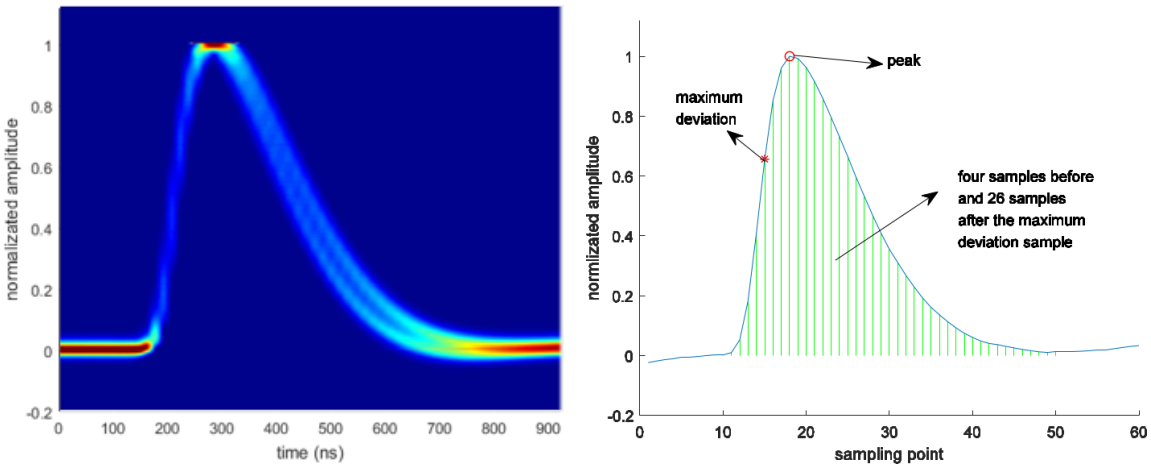

(a) (b)

Figure 2. Normalization pulse waveforms of the GAGG phoswich scintillator detector; (b) a pulse waveform.

2.2 Experiment

The scintillator detector module is placed in a black box. The SiPM-supplied voltage is 29 V and the working temperature is ~ 23°C. Waveforms were acquired with a ^{57}Co source (about 1.8 μCi) put on the top of the scintillator detector. Figure 2(a) shows normalized waveforms of the GAGG-F/GAGG-T phoswich detector in afterglow mode (the display mode in an oscilloscope). Energies of X, Y, and E are calculated by integrating four samples before and 26 samples after the maximum deviation sample [30]. Then, the Anger logic position of each gamma-ray event is generated. The ratio (r) of the pulse waveform integration value (four samples before and 36 samples after the maximum deviation sample) to pulse peak value as shown in figure 2(b) is utilized to determine the scintillator types. A bi-Gaussian mixture model as shown in equation (2.1) is used to fit the distribution curve of r. GAGG-F and GAGG-T scintillators are distinguished using the crossover point of two Gaussian curves. Then, the flood maps of GAGG-F and GAGG-T are produced using events with r below and up the cut value respectively. Crystal position maps for GAGG-F and GAGG-T arrays are created by a self-development automatic program [31], based on which, the energy spectrum of each scintillator is produced. Each energy spectrum is then fitted with a Gaussian function to retrieve the photoelectric peak (μ) and the energy resolution (FWHM=2.355σ/μ).

$$f(r) = A_1 \exp\left(-\frac{(r-u_1)^2}{2\sigma_1^2}\right) + A_2 \exp\left(-\frac{(r-u_2)^2}{2\sigma_2^2}\right) \tag{2.1}$$

2020 JINST 15 T04001

3 Results

3.1 Scintillator discrimination

The histogram of r with all the events acquired from the GAGG-F/GAGG-T phoswich detector block and its fitted result are shown in figure 3. The bi-Gaussian mixture model fitted result of the histogram is $A_1 = 13033$, $\mu_1 = 14.64$, $\sigma_1 = 0.68$, $A_2 = 13773$, $\mu_2 = 16.87$, $\sigma_2 = 0.85$. The intersection point of two Gaussian curves is 15.62 in this platform. The distinguish leads to a clear separation of two kinds of scintillators. The probability of GAGG-F being mis-classified as GAGG-T is 7.4%, and the probability of GAGG-T being mis-classified as GAGG-F is 7.0%.

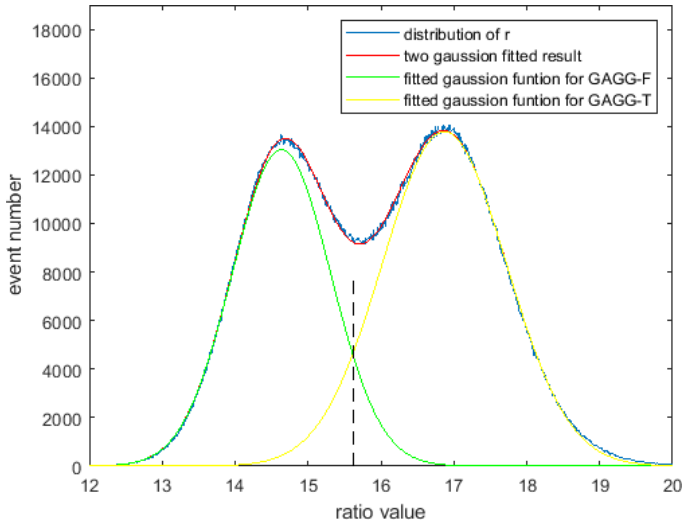

Figure 3. The distribution curve of r and its bi-Gaussian fitted result.

3.2 Position decoding

The ^{57}Co flood map ($\sim$ 5M events) of the phoswich detector has high overlap as shown in figure 4(a). After the discrimination of scintillator types, two flood maps including GAGG-F flood map ($r <$ 15.62) and the GAGG-T flood map ($r \geq$15.62) are generated as shown in figure 4(b)&(c). 12×12 scintillator array can be clear discriminated both in the GAGG-F and the GAGG-T flood maps. The flood maps have slight overlap at the border where the SiPM array has relative poor decodability. Experimental results indicate that the proposed detector has as intrinsic spatial resolution as the same size of the scintillator, i.e. 2.7×1.35 mm^2.

3.3 Energy resolutions

Figure 5(a) and (d) show the segmentation results of the GAGG-F flood map and the GAGG-T flood map respectively figure 5(b)&(e) illustrate photoelectric peaks of the 12×12 GAGG-F and 12×12 GAGG-T scintillators respectively. Figure 5(c)&(f) present energy resolutions of the 12×12 GAGG-F and 12×12 GAGG-T scintillators respectively. Figure 6 shows the typical spectra for GAGG-F scintillator and GAGG-T scintillator and their Gaussian fitted result. The average values

2020 JINST 15 T04001

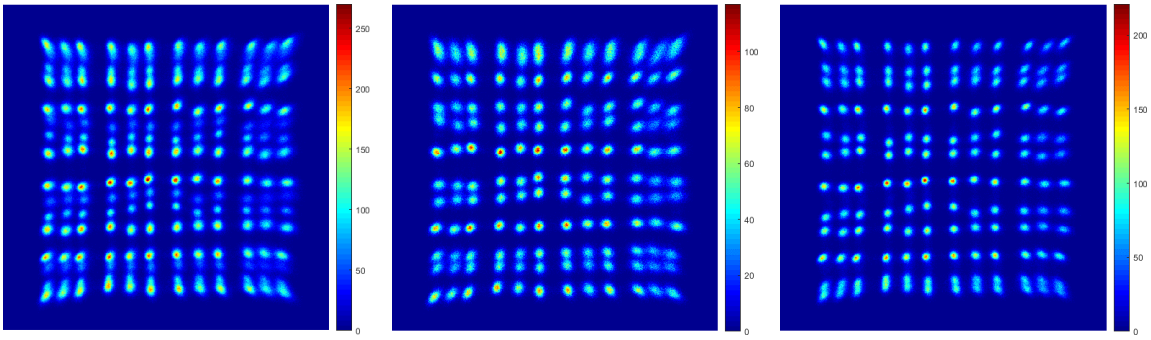

(a) (b) (c)

Figure 4. (a) GAGG-F/GAGG-T flood map, 2.7 mm pixel size in horizontal and 1.35 mm pixel size in vertical; (b) GAGG-F flood map ($r < 15.62$); (c) GAGG-T flood map ($r \geq 15.62$).

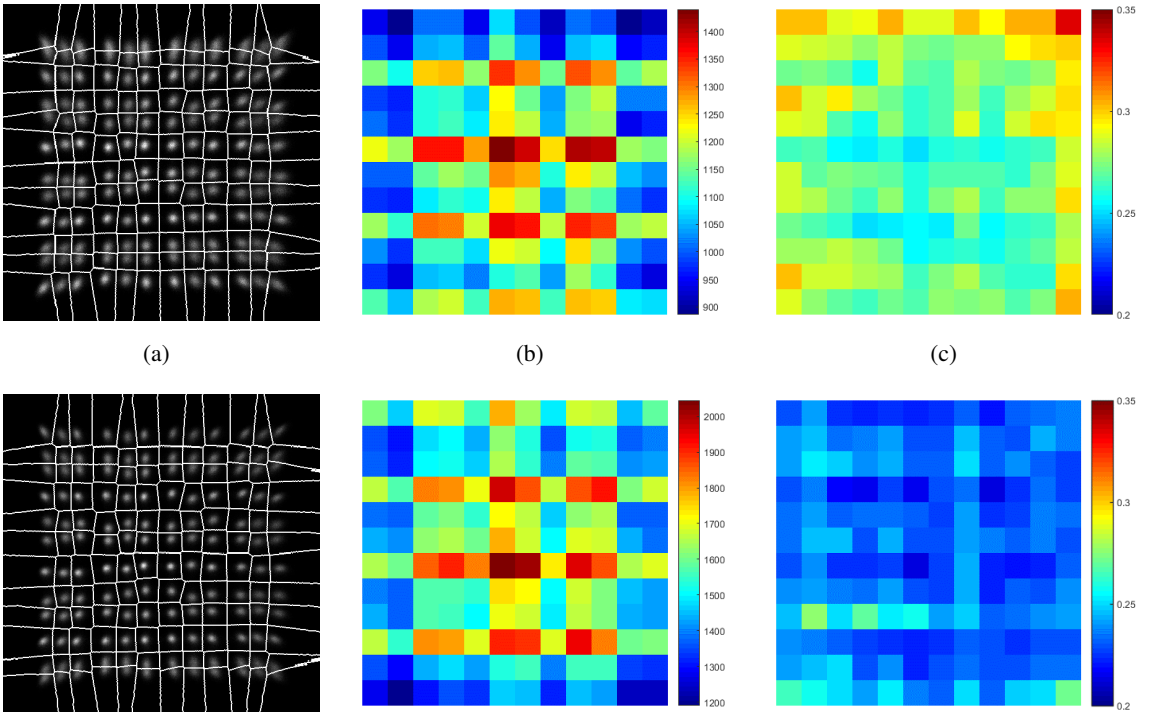

(a) (b) (c)

(d) (e) (f)

Figure 5. Results for the 12×12 GAGG-F array (row one) and the 12×12 GAGG-F array (row two): segmentation maps (a&d), photoelectric peaks at 122 keV (b&e), and energy resolutions at 122 keV (d&f).

and standard deviation values are given in table 2. The average photoelectric peaks of GAGG-F and GAGG-T scintillators at 122 keV are 1123±126 and 1569±179, respectively. The photo electric peak ratio of GAGG-F:GAGG-T is 0.72:1. The average energy resolutions of GAGG-F scintillators and GAGG-T scintillators at 122 keV are 27.58%±1.44% and 23.51%±1.07%, respectively.

2020 JINST 15 T04001

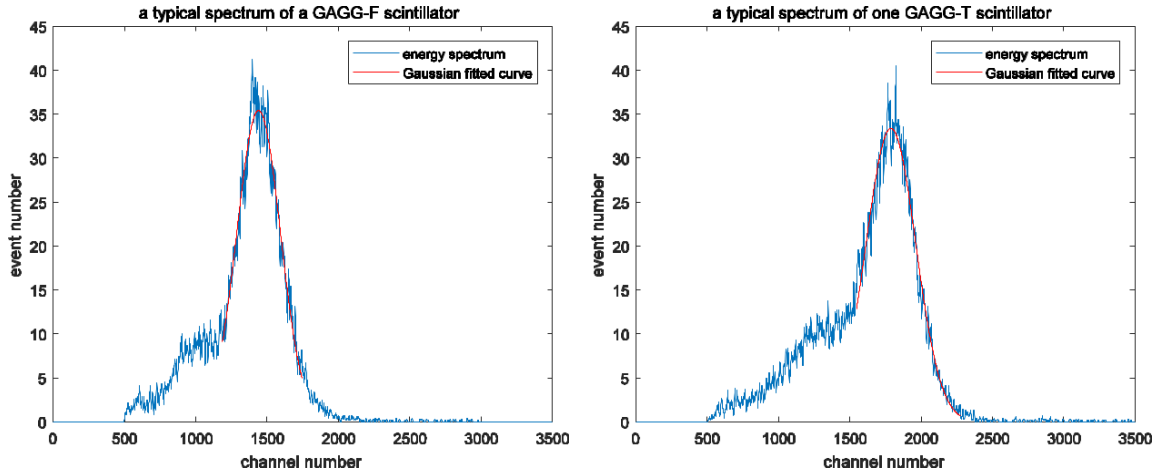

(a) (b)

Figure 6. Typical spectra of the GAGG-F scintillator (a) and GAGG-T scintillator (b).

Table 2. Result of average photoelectric peaks and average energy resolutions.

Scintillator	Average photoelectric peak	Average energy resolution
GAGG-F	1123±126	27.58%±1.44%
GAGG-T	1569±179	23.51%±1.07%

4 Discussion and conclusion

We have developed a gamma-ray position sensitive scintillation detector built with a side-by-side GAGG-F/GAGG-T phoswich scintillator array and decoded by a sparse SiPM array. We demonstrates that signals of GAGG-F and GAGG-T can be distinguished by using the ratio of the pulse integration value to pulse peak value. GAGG-F and GAGG-T scintillator arrays (12×12 for both) with 1.35×2.7×4 mm^3 pixels could be discriminated in separated flood maps. The average energy resolutions at 122 keV are 27.58% and 23.51% for 12×12 GAGG-F and 12×12 GAGG-T scintillators respectively.

Compared to our previous LYSO/GAGG phoswich design [14], the proposed GAGG-F/GAGG-T phoswich design has no intrinsic background radiation which can be used for low activity ECT imaging and coded-aperture cameras. Meanwhile, GAGG-F scintillator and GAGG-T scintillator have the same density and effective Z number, i.e. they have uniform detection efficiency which can make the normalization simply.

In conclusion, we developed a side-by-side GAGG-F/GAGG-T phoswich scintillation detector which has high intrinsic spatial resolution, no intrinsic background radiation and uniform detection efficiency. The proposed detector is suitable for high spatial resolution gamma-ray imaging systems.

2020 JINST 15 T04001

Acknowledgments

This work was supported in part by National Natural Science Foundation of China (Nos. 11975044 & 81727807), and in part by Fundamental Research Funds for the Central Universities (No. FRF-TP-19-019A3).

References

[1] S. Shifeng et al., *Far field 3D localization of radioactive hot spots using a coded aperture camera*, *Appl. Radiat. Isot.* **107** (2016) 177.

[2] M.J. Cieślak, K.A. Gamage and R. Glover, *Coded-aperture imaging systems: Past, present and future development — A review*, *Radiat. Meas.* **92** (2016) 59.

[3] T. Lee, H. Lee and W. Lee, *Coded aperture imager with depth of interaction scintillators*, *Nucl. Instrum. Meth.* **A 954** (2020) 161783.

[4] Q. Wei et al., *Performance evaluation of a compact PET/SPECT/CT tri-modality system for small animal imaging applications*, *Nucl. Instrum. Meth.* **A 786** (2015) 147.

[5] T. Dai et al., *A high-resolution small animal SPECT system developed at Tsinghua*, *Nucl. Sci. Tech.* **22** (2011) 344.

[6] Q.-Y. Wei et al., *Development of a compact DOI-TOF detector module for high-performance PET systems*, *Nucl. Sci. Tech.* **28** (2017) 43.

[7] F. Hueso-González et al., *Comparison of LSO and BGO block detectors for prompt gamma imaging in ion beam therapy*, 2015 *JINST* **10** P09015.

[8] H. Zhang et al., *Scintillation detector design study for prompt gamma photon detection in proton therapy monitoring*, in *2017 IEEE Nuclear Science Symposium and Medical Imaging Conference (NSS/MIC)*, IEEE, (Oct. 2017), DOI.

[9] B. Dolgoshein et al., *Status report on silicon photomultiplier development and its applications*, *Nucl. Instrum. Meth.* **A 563** (2006) 368.

[10] A. Del Guerra et al., *Silicon photomultipliers (SiPM) as novel photodetectors for PET*, *Nucl. Instrum. Meth.* **A 648** (2011) S232.

[11] M. Bergeron et al., *Performance evaluation of the LabPET APD-based digital PET scanner*, *IEEE Trans. Nucl. Sci.* **56** (2009) 10.

[12] Q. Wei, S. Wang, T. Ma, L. Lu, T. Dai and Y. Liu, *Design of a high resolution phoswich PET detector*, in *2011 IEEE Nuclear Science Symposium Conference Record*, IEEE, (Oct. 2011), DOI.

[13] S.K. Han, J. Yang, S. Hong and J. Kang, *Simulation study of side-by-side phoswich PET detector configuration for providing high spatial resolution of* $< 0.4\,mm$, in *2018 Joint 10th International Conference on Soft Computing and Intelligent Systems (SCIS) and 19th International Symposium on Advanced Intelligent Systems (ISIS)*, IEEE, (Dec. 2018), DOI.

[14] Q. Wei et al., *A side-by-side LYSO/GAGG phoswich detector aiming for SPECT imaging*, *Nucl. Instrum. Meth.* **A 953** (2020) 163242.

[15] Q. Wei, *Intrinsic Radiation in Lutetium Based PET Detector: Advantages and Disadvantages*, arXiv:1501.05372.

2020 JINST 15 T04001

[16] R. Yao, T. Ma and Y. Shao, *Lutetium oxyorthosilicate (LSO) intrinsic activity correction and minimal detectable target activity study for SPECT imaging with a LSO-based animal PET scanner*, *Phys. Med. Biol.* **53** (2008) 4399.

[17] K. Deprez, R.V. Holen and S. Vandenberghe, *A high resolution SPECT detector based on thin continuous LYSO*, *Phys. Med. Biol.* **59** (2013) 153.

[18] M. Vaiman et al., *Low-radiation of technetium-99m-sestamibi and single-photon emission computed tomography/computed tomography to diagnose parathyroid lesions*, *World J. Nucl. Med.* **18** (2019) 52.

[19] J.D. van Dijk, N.M. Borren, M. Mouden, J.A. van Dalen, J.P. Ottervanger and P.L. Jager, *Effect of a patient-specific minimum activity in stress myocardial perfusion imaging using CZT-SPECT: Prognostic value, radiation dose, and scan outcome*, *J. Nucl. Cardiol.* **25** (2017) 26.

[20] Q. Ye et al., *A high sensitivity 4π view gamma imager with a monolithic 3d position-sensitive detector*, *Nucl. Instrum. Meth.* **A 937** (2019) 31.

[21] K. Nakanishi, S. Yamamoto and J. Kataoka, *Performance comparison of finely pixelated LYSO- and GAGG-based Si-PM gamma cameras for high resolution SPECT*, *Nucl. Instrum. Meth.* **A 872** (2017) 107.

[22] S. Yamamoto, J.Y. Yeom, K. Kamada, T. Endo and C.S. Levin, *Development of an ultrahigh resolution block detector based on 0.4 mm pixel ce:GAGG scintillators and a silicon photomultiplier array*, *IEEE Trans. Nucl. Sci.* **60** (2013) 4582.

[23] R. Wang et al., *Absolute gamma source positioning with position-sensitive scintillation detector arrays*, in *2018 IEEE Nuclear Science Symposium and Medical Imaging Conference Proceedings (NSS/MIC)*, IEEE, (Nov. 2018), DOI.

[24] W. Chewpraditkul et al., *Scintillation properties of gd3al2ga3o12:ce, li and gd3al2ga3o12:ce, mg single crystal scintillators: A comparative study*, *Opt. Mater.* **92** (2019) 181.

[25] S. Yamamoto et al., *Development of GAGG depth-of-interaction (DOI) block detectors based on pulse shape analysis*, *Nucl. Instrum. Meth.* **A 767** (2014) 289.

[26] P. Sibczynski et al., *Characterization of GAGG:ce scintillators with various al-to-ga ratio*, *Nucl. Instrum. Meth.* **A 772** (2015) 112.

[27] Q. Wei et al., *Performance evaluation of a PET detector with a sparse SiPM array and gap reflectors* (in Chinese), *J. Tsinghua Univ. (Sci. & Technol.)* **58** (2018) 929.

[28] X. Zhu et al., *Development of a 64-Channel Readout ASIC for an 8×8 SSPM Array for PET and TOF-PET Applications*, *IEEE Trans. Nucl. Sci.* **63** (2016) 1327.

[29] http://www.epic-crystal.com/.

[30] Q. Wei, T. Ma, T. Xu, Y. Liu, S. Wang and Y. Gu, *Evaluation of signal energy calculation methods for a light-sharing SiPM-based PET detector*, *Nucl. Instrum. Meth.* **A 848** (2017) 81.

[31] Q. Wei, T. Dai, T. Ma, Y. Liu and Y. Gu, *Crystal identification in dual-layer-offset DOI-PET detectors using stratified peak tracking based on SVD and mean-shift algorithm*, *IEEE Trans. Nucl. Sci.* **63** (2016) 2502.

2020 JINST 15 T04001